

FLOW IN A MODEL ROCKET NOZZLE

C.W. Hirt
Flow Science, Inc.
3/11/89

OVERVIEW

In a previous technical note, FSI-89-TN17, "Flow in a Solid-Propellant Rocket Chamber," calculational results were presented for the turbulent flow in the interior of a "cold flow" model of a solid propellant rocket. For the interior flow calculations the nozzle of the rocket was omitted from the analysis and replaced by a specified pressure boundary condition a short distance upstream of the nozzle entrance.

Omitting the nozzle from the previous study was a matter of expediency. Initial attempts to include the nozzle in that analysis failed because the desired steady-state pressure within the rocket chamber could not be maintained. It was surmised that the reason for this failure was insufficient resolution of the large flow gradients in the vicinity of the nozzle throat.

This note describes a more detailed investigation of the rocket-nozzle region. The results obtained here do confirm that limited resolution was the source of difficulty with the original calculations.

A secondary purpose of this note is to demonstrate and compare the use of two different upstream boundary conditions. One condition is based on a specified upstream pressure. The alternative condition assumes a specified flow rate at the upstream boundary. In both cases a two-equation turbulence model has been used to approximate turbulent flow effects.

COMPUTATIONAL MODEL

The rocket chamber is axisymmetric with an internal radius of 2.0 inches. As described in the previous note, nitrogen gas is injected into the chamber through porous walls to simulate the production of gas at the surface of the burning solid propellant. The original design called for a steady-state chamber pressure of 30.0 psi at 500 R. The main cylindrical chamber is 29.0 inches in length with gas injection occurring over the first 28.5

inches. By injecting gas at a rate equal to the rate predicted by one-dimensional theory for critical flow through the nozzle, it should be possible to establish steady flow conditions at the designated chamber pressure.

The nozzle of the rocket consists of a 30° cone section blended with a toroidal-shaped throat. The throat (i.e., the center of the torous) has a radius of 0.695 inches. Figure 1 shows a sketch of the basic geometric arrangement and the subregion to be modeled.

To model the flow in the nozzle region, a computational mesh was generated that started 1.5 inches upstream of the conical insert and extended 0.545 inches downstream of the minimum throat area location. The mesh and obstacle setup used in the first calculation is shown in Fig. 2. It consists of 16 cells in the radial direction and 23 cells in the axial direction. Seven (7) of the 16 radial cells have been located in the throat, and the axial cell sizes in this region have been made smaller to provide better resolution where larger flow gradients are expected.

All calculational results presented below have been obtained with FLOW-3D using the full compressible flow option and with the two-equation, K-Epsilon, turbulence model. The implicit, ICE method for pressure-velocity coupling was used to insure computational stability in the upstream, far subsonic region of the flow.

Inflow conditions for the turbulence at the upstream boundary of the mesh were uniform with values equal to about one half of the maximum values computed in the interior-flow study. No attempt was made to use the previously computed distributions of quantities at the upstream boundary because the velocities there were more than an order of magnitude smaller (Mach 0.09) than the supersonic velocities generated in the nozzle.

The downstream, outflow boundary was specified to be a specified pressure boundary at atmospheric pressure 14.7 psi and temperature 500 R. Since the flow is supersonic at the outflow, the actual boundary conditions used there are not critical as they cannot influence the upstream flow.

A complete input data file for the first calculation to be described in the next section is given in Fig. 3. This includes the equation of state data for nitrogen (a polytropic gas) with initial conditions consisting of 30 psi gas at rest and having a temperature of 500 R.

COMPUTATIONAL RESULTS

Three calculations are reported in this note. In the first example a modest grid resolution was used with a specified pressure condition at the upstream boundary. Because the computed flow rate was found to be higher than expected, two additional calculations were then performed to investigate possible reasons for the discrepancy.

Specified Pressure Case

At the upstream (bottom) end of the computational region the pressure was input to be the desired 30 psi chamber pressure. Additionally, PBCTYP=1 was set so that this pressure would be interpreted as a stagnation pressure condition.

Starting from rest, the flow evolved in time to a time of 0.007 s. A time history of total mass in the computational region, Fig. 4, indicates that steady flow conditions were reached in this time interval. The calculation took 3047 time cycles and required 7.11 hours of CPU time on a MicroVAX II computer.

Figure 5 contains the computed steady-state velocities, pressures and temperatures. Corresponding turbulence quantities, i.e, turbulence energy, dissipation and dynamic viscosity, are shown in Fig. 6.

A theoretical calculation of critical conditions occurring at the Mach 1.0 surface, with respect to the upstream stagnation conditions, gives:

$$p = 0.528p_0 = 15.848 \text{ psi}$$

$$T = 0.833T_0 = 414^\circ \text{ R}$$

$$c = 0.913c_0 = 1.224\text{E}+4 \text{ in/s}$$

$$\rho = 0.634\rho_0 = 1.778\text{E}-6 \text{ slugs/in}^3$$

In Fig. 5 the contours marked by an arrow along the left side of the plots are very close to the critical contour values.

At the minimum area location in the nozzle throat the axial velocity is seen to be slower at the centerline than it is at the surface of the nozzle. This observation is consistent with the shapes of the critical isobar and isotherm, which indicates that sonic conditions are reached in the minimum area section only at

the wall of the nozzle. Two-dimensional effects associated with flow convergence in the nozzle push the critical surface on the centerline downstream of the minimum area location.

In Fig. 6 we observe that the turbulence energy and dissipation are largest in the throat region and near the nozzle wall. This is to be expected since the shear stresses are greatest in this region. The dynamic viscosity, however, exhibits a maximum somewhat away from the nozzle wall and is three orders of magnitude larger than the molecular viscosity.

The computed mass flow rate through the nozzle was found to be $3.00E-3$ slugs/s. The theoretical flow rate based on a one-dimensional analysis is $2.76E-3$ slugs/s. Thus, the calculated rate is 8.7% higher than the theoretical value. This is consistent with the results of the full rocket chamber calculations, which exhibited too large a mass flow rate through the nozzle.

The discrepancy in mass flow rate could be the result of several factors. For instance, the one-dimensional theory does not account for a two-dimensional flow profile in the nozzle or for the influence of turbulence, which were effects included in the computations. Unfortunately, both of these effects are likely to reduce the computed flow rate rather than increase it. Another possibility is that the method used to set the upstream, stagnation-pressure, boundary conditions is inaccurate. Finally, it is also possible that insufficient numerical resolution was available to accurately resolve the rapid flow changes occurring in the nozzle region.

The last two hypotheses can be easily tested by additional computations. For instance, the question of the upstream boundary treatment can be investigated by replacing the pressure condition with an alternative flow rate condition. To address the question of resolution, a finer grid must be used in the nozzle region.

Specified Flow Rate Case

To study the influence of the upstream boundary condition, a second computation was performed that had a specified flow rate defined at the upstream boundary. For this purpose the inflow velocity was set uniformly across the boundary to give the one-dimensional theoretical mass flow rate. The calculation was then carried out to a time of 0.007 s as before, which required 3017 time cycles and 6.72 hours of CPU time on a MicroVAX II computer. A review of the total mass history and other global quantities in the mesh indicated that the results were at steady state

conditions by the end of the computation.

Output from this second case is displayed in Figs. 7-8. The overall results are qualitatively similar to those obtained in the first case, except that the average pressure upstream of the nozzle is now 27.5 psi and not the 30 psi that was expected. This finding is consistent with the previous case, at least in the sense that the computations and the one-dimensional theory are not consistent with one another. The lower flow rate specified in this case is also consistent with the lower upstream pressure.

Higher Resolution Case

Reference to Fig. 5 indicates that the principal flow gradients are in the axial direction in the entrance region to the nozzle, i.e., where cross sectional area changes are greatest. Thus, the greatest gain in accuracy is expected to arise from a reduction in the axial cell size in this region. Fig. 9 shows a refined mesh based on this idea and the corresponding input file used for the third, and last, calculation. The cell resolution in the high gradient region has been increased by about a factor of 1.5, while the total number of grid cells has been increased by a factor of 1.37.

In this calculation the specified pressure condition used in the first case was again used at the upstream boundary. The calculation took 5663 cycles to reach a final time of 0.007 s, at which time it was confirmed that the results had reached steady conditions. A significantly longer CPU time of 17.1 hours was required to complete the calculation. The larger time reflects a larger mesh size (i.e., greater number of cells) and smaller time-step size needed to maintain computational stability.

Computed results from the higher resolution case are given in Figs. 10-11. Arrows at the left edges of the contour plots again mark the locations of the critical values. The computed mass flow rate was $2.78E-3$ slugs/s, which is now only 0.7% higher than the one-dimensional theoretical prediction. Clearly, even the modest increase in grid resolution used here has made a big improvement in the computed results.

A comparison of Figs. 10-11 with the earlier results shown in Figs. 5-6 reveals a strong qualitative similarity except for the turbulence energy and dissipation contour plots. In Fig. 11 there appears to be a locally high concentration of turbulence along the nozzle wall just downstream of its minimum area. The maximum values are about a factor of three larger than the corresponding values in the earlier calculation. It is believed that this happens because of the boundary condition treatment of

turbulence quantities as discussed in the companion technical note, TN17. The dynamic viscosity, which is formed from a combination of the other quantities, is not significantly affected by this difference because the boundary treatment was designed to produce a reasonable viscous wall shear stress. Furthermore, since velocities and other mean flow variables are only influenced by the resultant viscosity, they should not be significantly affected either.

SUMMARY

Several calculations have been described that model the transition from subsonic to supersonic flow in a model rocket nozzle. The first two calculations used different upstream boundary conditions - a specified pressure condition in the first case and a specified flow rate in the second. In both cases the computed results exhibited discrepancies on the order of 8% with respect to theoretical predictions.

A third calculation was then performed using a more refined grid in the convergence region of the nozzle. This example differed by less than 1% from the theoretical predictions and confirms that the less accurate results obtained in the first two calculations were caused by poor resolution and not by the choice of upstream boundary condition. With the increased resolution FLOW-3D is producing good results for the nozzle flow problem.

The computational results closely agree with the one-dimensional predictions for flow rate. They additionally provide a flow profile in the nozzle that is not available from the theory, and they show that turbulence effects do not significantly alter the flow rate.

Based on these findings we may conclude that a complete calculation of a solid rocket, i.e., chamber plus nozzle, is possible but will require good resolution in the nozzle region in order to achieve the proper balance between the gas source rate and the critical mass flow rate through the nozzle. Such a calculation would be best performed on a computer that is significantly faster than a MicroVAX II computer.

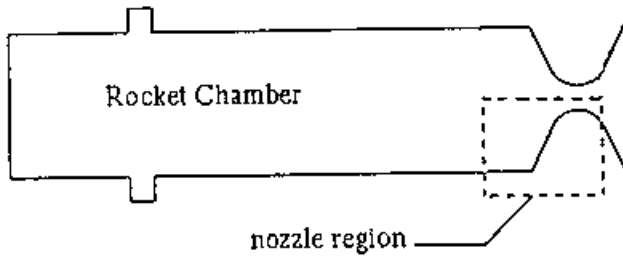


Fig. 1. Sketch of rocket geometry. Dashed box indicates region modeled.

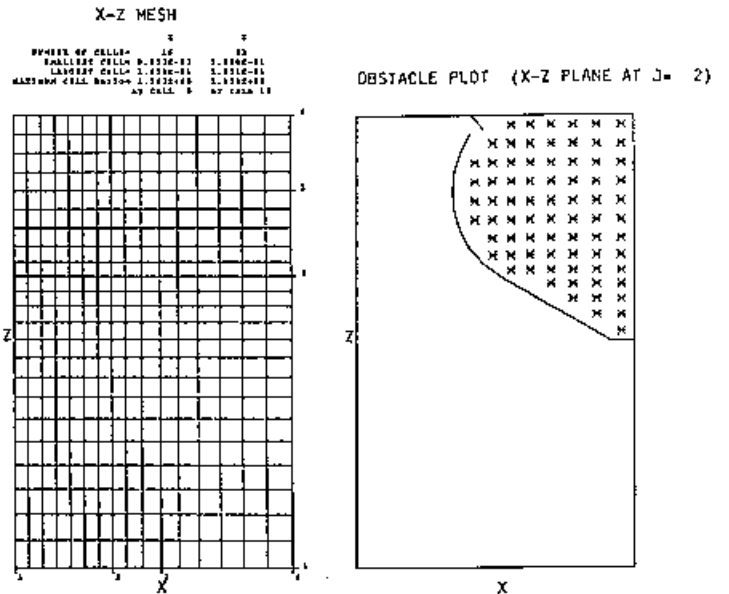


Fig. 2. Mesh and obstacle arrangement.

```

COLD FLOW - NOZZLE
$XPUT
  ICMPRS=1,      IFVIS=3,      IWSH=1,
  CYL=1.0,      AVRCK=-2.1,     ALPHA=.5,
  NR=2,         WB=5,         WT=5,
  PBCT(1,5)=30., FBCT(1,5)=0.0, TBCT(1,5)=500.,
  TRDCT(1,5)=-2.62E+4, DTRBCT(1,5)=1.13E+7,
  PBCT(1,6)=14.7, FBCT(1,6)=0.0, TACT(1,6)=500.,
  RMRHO=1.0,    RMRHOE=1.0,   MUI=2.61E-9,
  CV2=6.416E+5, RF2=2.566E+5, EPSI=.03,
  DELT=1.0E-5,  CON=.25,      PLTDT=.003,  PRTDI=.025,
  TWFIN=.007,   TLEN=0.0414,
  TKEI=2.62E+4, PBCTYP=1.0,
  IRFR=9,      MBPR=19,      XTFR=22,

$END
$MESH
  NXCELL=16,    FX(3)=1.045,    FX(4)=2.0,
  FX(2)=0.695,  NXCELL(1)=7,      NXCELL(2)=3,
  SIZEX(2)=0.1,
  NYCELL=1,
  PY(2)=1.83,
  NZCELL=23,
  PZ(1)=-27.5,  PZ(2)=-29.5514,  PZ(3)=30.157,  PZ(4)=30.7,
  SIZEZ(2)=0.1,  NZCELL(2)=5,

$END
$OBS
  NOBS=1,
  IOFO(1,1)=-1,  CRXY(1)=-.5775,  CC(1)=30.155,  CZ(1)=-1.0,
  IOFO(2,1)=-2,  CRXY(2)=-2.79,  CC(2)=910.901,  CZ2(2)=1.,
  CZ(2)=-60.314,  RAH(2)=-1.045,
  CZ2(2)=-1.,

$END
$PL
  PRSSI=30.,

$END
$BP
$END
$TEMP
  TEMPI=500.,

$END
$GRAFIC
  NVPLTS=1,      KVE(1)=24,
  NCPLTS=4,
  KONTYP(1)=9,   KC2(1)=24,
  KONTYP(2)=10,  KC2(2)=24,
  KONTYP(3)=11,  KC2(3)=24,   KC2(4)=24,
  ILOC(1)=2,     JLOC(1)=2,   KLOC(1)=21,

$END
$PARTS
$END

```

Fig. 3. Input file for first calculation.

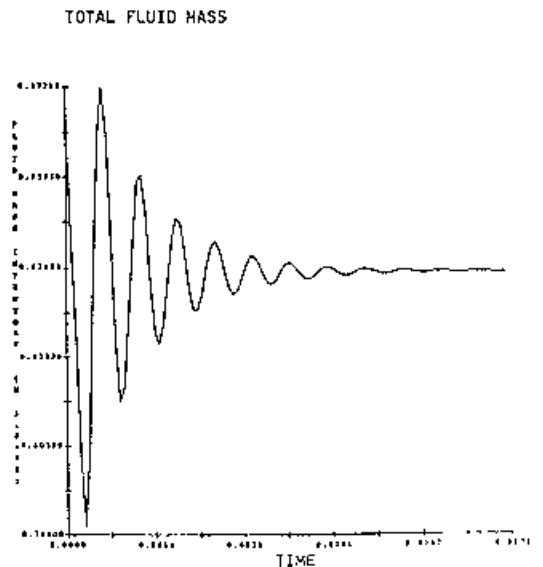


Fig. 4. Time history of total fluid mass in computational region.

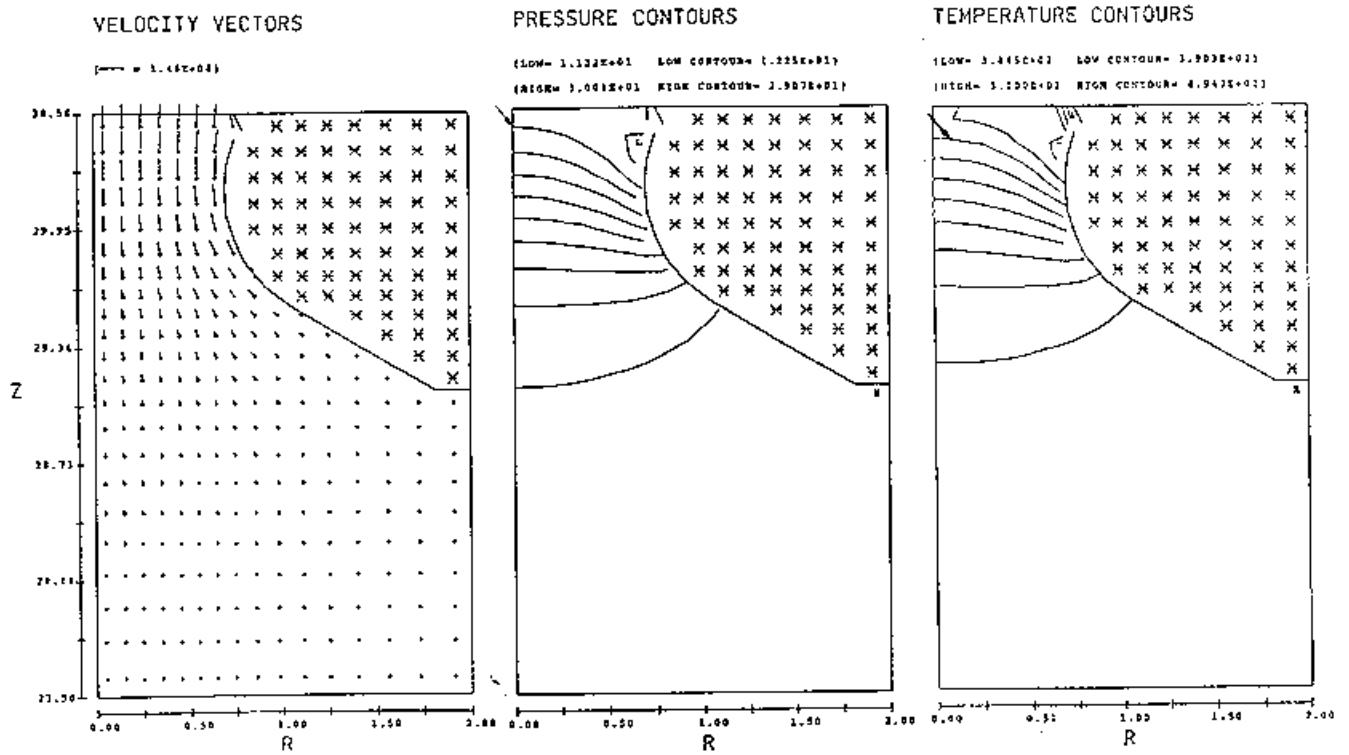


Fig. 5. Steady state results for mean flow quantities in problem one.

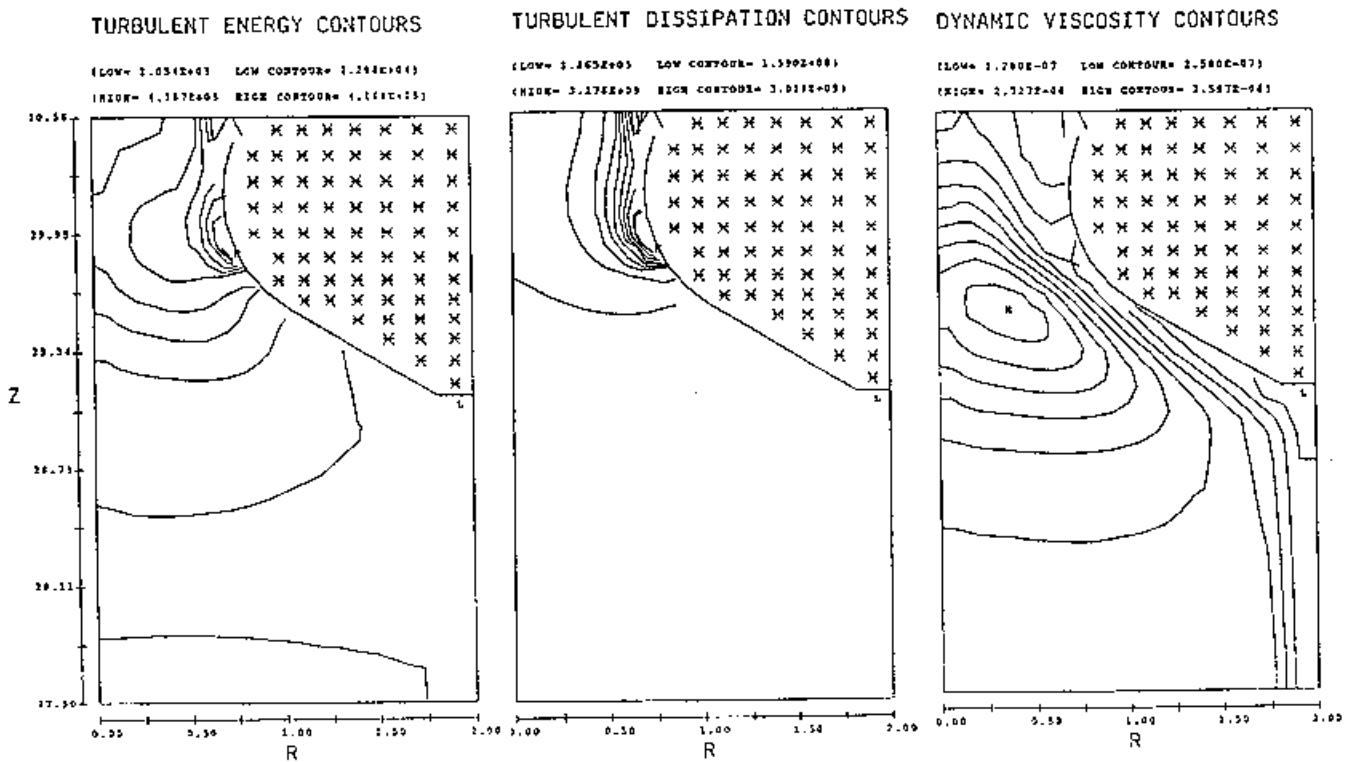


Fig. 6. Steady state results for turbulence quantities in problem one.

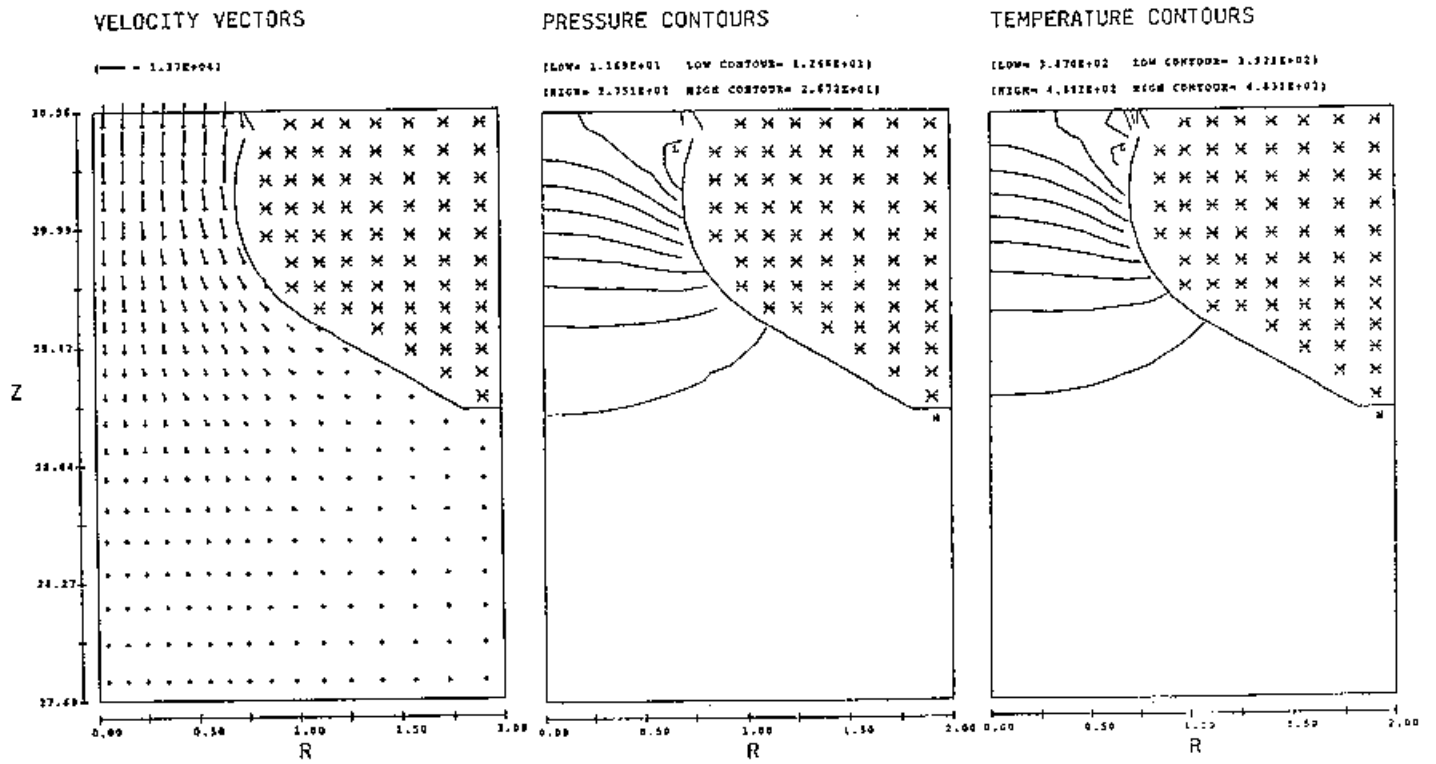


Fig. 7. Steady state results for mean flow quantities in problem two.

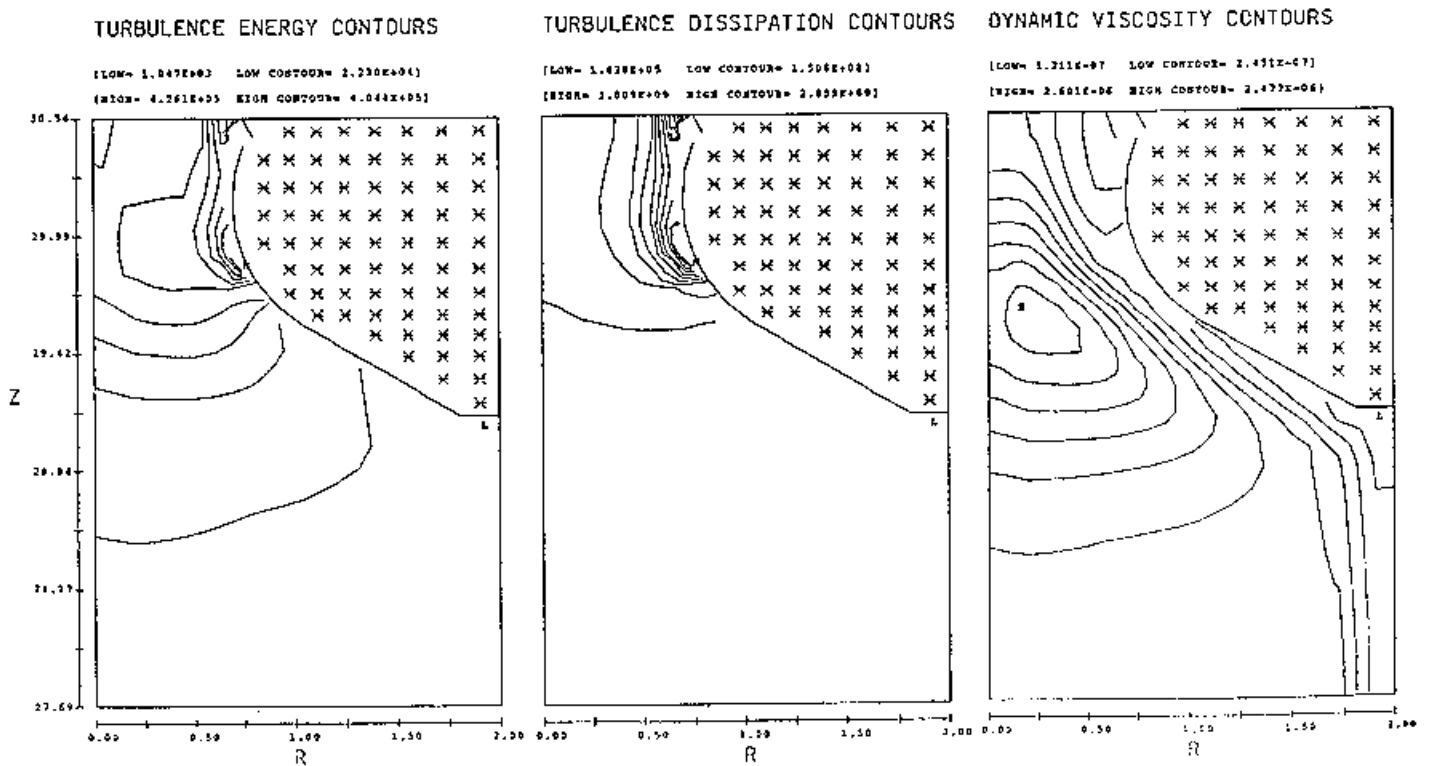


Fig. 8. Steady state results for turbulence quantities in problem two.

COLO FLOW - NOZZLE HI-REZ

```

$XPUT
  ICMPRS=1,      IFVIS=3,      IWSH=1,
  CYL=1.0,      AVRCK=-2.1,     ALPHA=.5,
  WR=2,         WB=5,         WT=5,
  PBCT(1,5)=30., FBCT(1,5)=0.0, TBCT(1,5)=500.,
  TRBCT(1,5)=2.62E+4, DTRBCT(1,5)=1.13E+7,
  PBCT(1,6)=14.7, FBCT(1,6)=0.0, TBCT(1,6)=500.,
  RMRHO=1.0,    RMRHOE=1.0,
  CV2=6.416E+5, RF2=2.566E+5, MUI=2.61E-9,
  DELT=0.50E-5, CON=.25,     EPSI=.03,
  TWFIN=.007,   FLTDT=.003,   PRDTE=.025,
  TKEI=2.62E+4, TLEN=0.0414,
  PBCTYP=1.0,
  IRPR=9,      KBPR=19,      KTRP=22,

$END
$MESH
  NXCELLT=18,
  PX(2)=0.645,    PX(3)=1.045,    PX(4)=2.0,
  SIZEX(2)=0.1,  NXCELL(1)=7,   NXCELL(2)=4,
  NYCELLT=1,
  PY(2)=1.83,
  NZCELLT=28,
  PZ(1)=27.5,    PZ(2)=29.5514, PZ(3)=30.157, PZ(4)=30.7,
  SIZEZ(3)=0.07, NZCELL(2)=7,  NZCELL(3)=6,

$END
$OBS
  NOBS=1,
  IOFO(1,1)=1,   CRXY(1)=-.5775,  CC(1)=30.155,  CZ(1)=-1.0,
  IOFO(2,1)=2,   RAL(1)=1.045,      CRXY(2)=-2.79, CC(2)=910.901, CZ2(2)=1.,
  C2(2)=-60.314, CX2(2)=1.,  RAH(2)=1.045,

$END
$FL
  PRESI=30.,

$END
$BF
$END
$TEMP
  TEMPI=500.,

$END
$GRAPHIC
  NVPLTS=1,      KV2(1)=29,
  NCPLTS=5,
  KONTP(1)=9,    KC2(1)=29,
  KONTP(2)=10,   KC2(2)=29,
  KONTP(3)=11,   KC2(3)=29,    KC2(5)=29,
  KONTP(4)=5,    KC2(4)=29,
  ILOC(1)=2,     JLOC(1)=2,    RLOC(1)=24,

$END
$PARTS
$END

```

X-Z MESH

	X	Z
NUMBER OF CELLS=	14	28
SMALLEST CELL=	8.429E-02	7.000E-02
LARGEST CELL=	1.729E-01	1.705E-01
MAXIMUM CELL RATIO=	1.121E+00	1.117E+00
	AT CELL 13	AT CELL 25

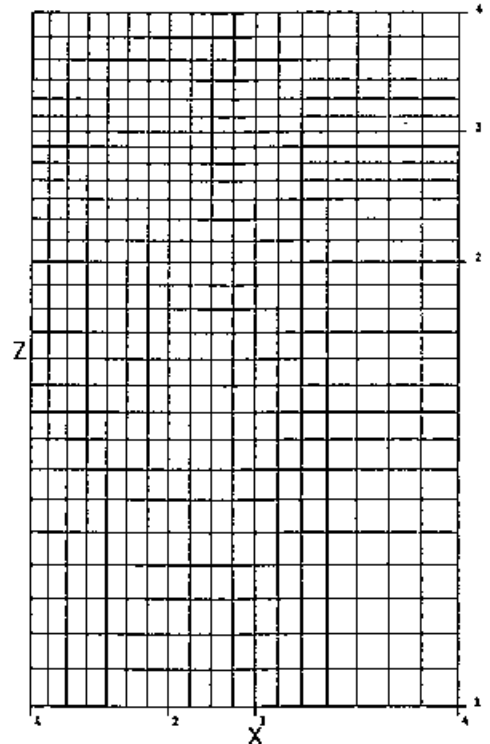


Fig. 9. Mesh and input file for highest resolution case.

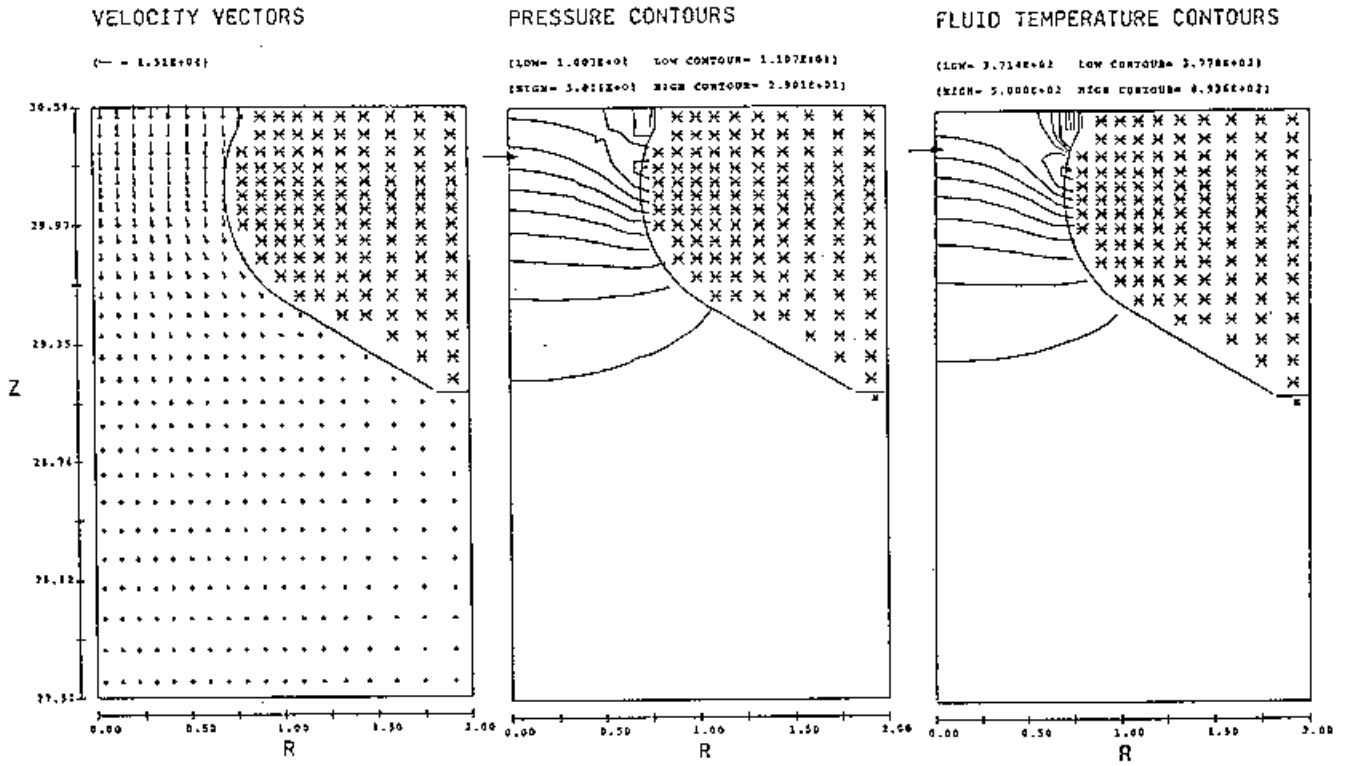


Fig. 10. Steady state results for mean flow quantities in problem three.

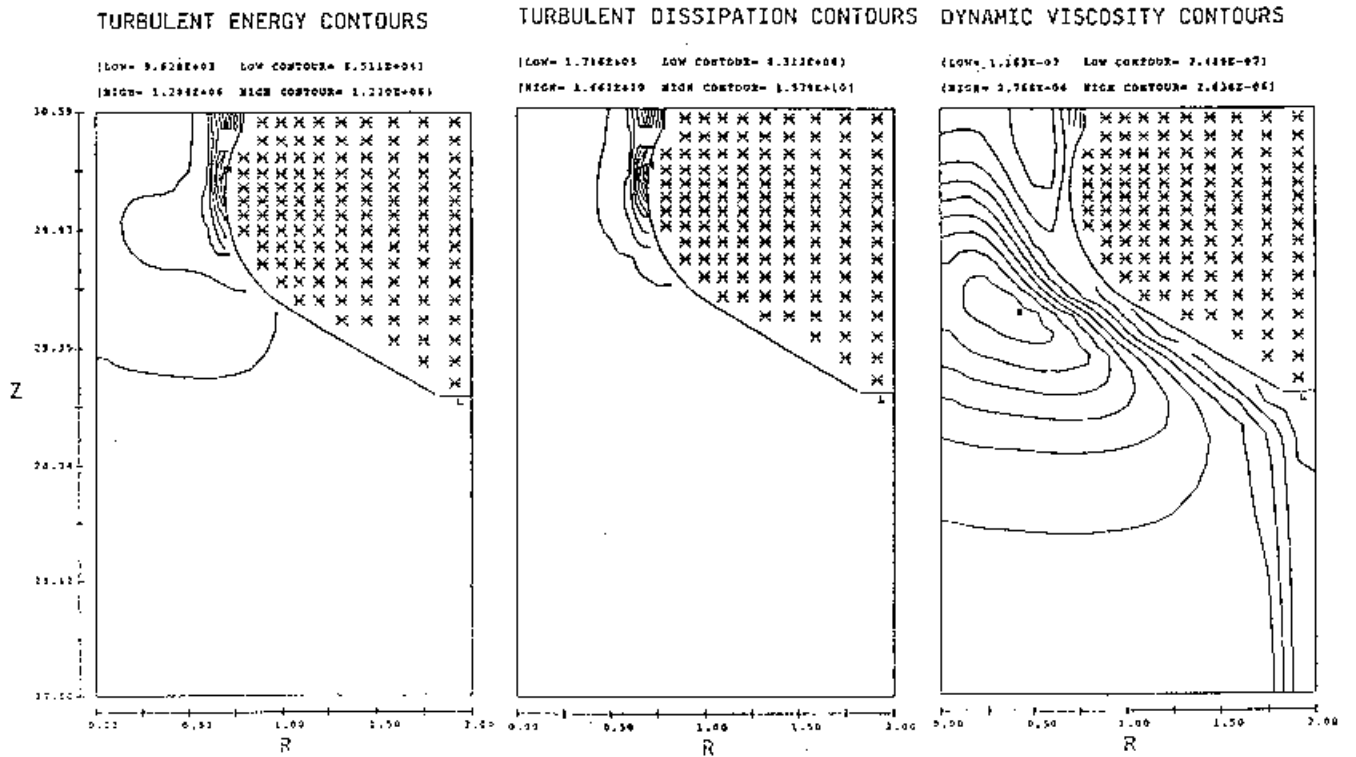


Fig. 11. Steady state results for turbulence quantities in problem three.